Line shape of the Cr^{3+} luminescence in garnet crystals

M. Yamaga
Department of Physics, Faculty of General Education, Gifu University, Gifu 501-11, Japan

B. Henderson and K. P. O'Donnell
Department of Physics and Applied Physics, University of Strathclyde, Glasgow G4 ONG, United Kingdom
(Received 29 July 1991; revised manuscript received 4 December 1991)

The line shapes of Cr^{3+} photoluminescence in garnet crystals, in which the ^2E and $^4T_2$ excited states are close in energy, have been calculated with use of the vibronic tunneling model developed previously by the present authors. At low temperatures, the experimental luminescence spectrum from Cr^{3+} in $Y_3Ga_5O_{12}$, $Gd_3Sc_2Al_3O_{12}$, and $Gd_3Sc_2Ga_3O_{12}$ is always an admixture of $^2E \rightarrow {}^4A_2$ and $^4T_2 \rightarrow {}^4A_2$, the relative amounts being determined by the energy difference $\Delta E = E(^4T_2) - E(^2E)$. The line shapes, calculated in terms of mixing of ^2E and $^4T_2$ adiabatic vibronic wave functions via spin-orbit and nuclear kinetic-energy operators, reproduce the experimental low-temperature spectra rather well. Our calculation of the temperature dependence of the Cr^{3+}:$Gd_3Sc_2Al_3O_{12}$ line shape agrees with the experimental spectra.

I. INTRODUCTION

The mixed oxide garnets $A_3B_2C_3O_{12}$ are ideal host lattices in which to study the optical-absorption and emission spectra of trivalent transition-metal ions. Such ions prefer to occupy octahedral B^{3+} sites, which undergo weak trigonal distortions. Interest in these materials is related to their potential as tunable laser gain media operating at room temperature. The strength of the octahedral crystal field in these hosts may be varied in a systematic way through the size of the unit cell and, thereby, the chemical composition. For example, along the series in which the A^{3+} site is occupied by Y^{3+}, Gd^{3+}, or La^{3+}, the octahedral field weakens progressively. Similarly, a monotonic diminution of the octahedral field occurs along the series in which Al^{3+}, Ga^{3+}, or Sc^{3+} ions occupy the B^{3+} site.

Whether the ^{2}E or $^4T_2$ level is the lowest, resulting in sharp line or broadband emission, respectively, is determined by the strength of the crystal field. The ordering of these excited levels of Cr^{3+} in garnets such as $Y_3Al_5O_{12}$ (YAG), $Y_3Ga_5O_{12}$ (YGG), $Gd_3Ga_5O_{12}$ (GGG), $Gd_3Sc_2Al_3O_{12}$ (GSAG), $Gd_3Sc_2Ga_3O_{12}$ (GSGG), and $La_3Lu_2Ga_3O_{12}$ (LLGG) depends on whether the crystal field is weak, in which case $\Delta E = E(^4T_2) - E(^2E) < 0$, or strong, where $\Delta E > 0$.[1] The luminescence spectra of Cr^{3+} ions in these materials, as discussed by the authors[2-8] and others,[1,9-13] are also complicated by Cr^{3+} multisites associated with nonstoichiometry.[1,6,7,12] Variations in crystal-field strength in the presence of compositional disorder lead to interesting spectral variations in both wavelength and time domains.

Sharp R-line emission, due to the $^2E \rightarrow {}^4A_2$ multiplicity-forbidden transition, is allowed by mixing of the $^4T_2$ and ^2E electronic states through spin-orbit coupling.[14,15] In ruby, where $Dq/B \sim 2.8$, the observed emission is in the R line, even at 300 K. A contrast is found with LLGG, where $^4T_2$ is lowest: At room temperature the observed emission is then the broad $^4T_2 \rightarrow {}^4A_2$ luminescence band.[1] The gadolinium-based garnets GSGG and GSAG are interesting because the energy difference between ^2E and $^4T_2$ is small; as a consequence, the emission line shape is a mixture of R-line and broadband processes, even at 4.2 K.[1,2] For Cr^{3+}:GSGG and Cr^{3+}:GSAG, the room-temperature luminescence is predominantly the broad $^4T_2 \rightarrow {}^4A_2$ band. Both materials are suitable for use as gain media in tunable solid-state laser operating at room temperature. Nonradiative decay processes hardly affect the radiative decay time and the emission intensity below room temperature: These effects appear in the emission spectra at higher temperature ($T > 500$ K).[16] Unfortunately, the slope efficiency of these Cr^{3+}-garnet lasers is strongly reduced relative to, e.g., the alexandrite laser as a consequence of excited-state absorption of both excitation and emission radiation.[17,18]

Recently, the authors have solved the vibronic Hamiltonian appropriate to the Cr^{3+}-garnet case in the Born-Oppenheimer (BO) adiabatic approximation: The inclusion of spin-orbit coupling as a perturbation on the electronic terms mixes different ^2E and $^4T_2$ electronic levels with the same nuclear configuration, whereas the electron-vibrational coupling includes an electronic operator that mixes levels with different configurations.[2] These mixings result, respectively, in vertical and horizontal tunnelings between the levels.[2,19] The theory gives an excellent theoretical fit to the observed intensities and luminescence decay times for ^2E and $^4T_2$ states as a function of temperature for Cr^{3+} ions in the garnets YGG, GSAG, and GSGG.[3,4]

The present paper describes the ^2E and $^4T_2$ vibronic wave functions of Cr^{3+} ions, for which the ^2E and $^4T_2$ energy levels are very close, using mixed-spin BO basis sets.[20-22] The line shape of the Cr^{3+} luminescence is then calculated in terms of the lowest vibronic wave functions

and compared with the experimental line shapes in YGG, GSAG, and GSGG. The theory is shown to account for the material-by-material variations in luminescence behavior of Cr^{3+} ions in ionic crystals. Furthermore, the temperature dependence of the Cr^{3+}:GSAG emission line shape is also calculated and compared with the experimental results. Such a calculation is important in accounting for the room-temperature operation of lasers based on Cr^{3+}-doped garnets, in particular their broadband tuning range. Nonradiative decay processes hardly affect the radiative decay time and the emission intensity below room temperature: These effects appear in the emission spectra at higher temperature ($T > 500$ K).[16,17] Indeed, the primary process resulting in a decrease in the slope efficiencies of the GSGG and GSAG lasers is excited-state absorption of the broad emission band.[17,18]

II. THEORY

A. ^2E and $^4T_2$ vibronic states of Cr^{3+}

Radiationless transitions due to intersystem crossing between multiplet spin states in polyatomic molecules have been discussed by several authors in terms of a vibronic Hamiltonian including as perturbations spin-orbit coupling and nuclear kinetic-energy operators.[20–27] This paper applies this vibronic Hamiltonian to the energy levels of Cr^{3+} ions in garnet crystals. Figures 1(a) and 1(b), respectively, show the electronic energy levels of Cr^{3+} in octahedral symmetry and on a single-configuration coordinate diagram. The arrows in Fig. 1(a) indicate transitions allowed through spin-orbit coupling between the electronic states. In the BO adiabatic approximation, the ^2E and $^4T_2$ excited vibronic states of Cr^{3+} are separated by a potential barrier, as shown in Fig. 1(b). When the energy levels of the ^2E and $^4T_2$ vibronic excited states of Cr^{3+} are almost degenerate, the adiabatic approximation breaks down, and the states are mixed by the combined action of spin-orbit coupling and nuclear kinetic-energy operators including zero-point vibrations.

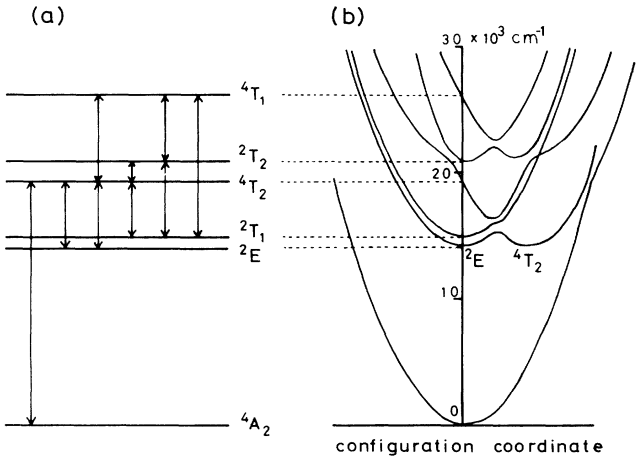

FIG. 1. (a) Energy levels of the Cr^{3+} ($3d^3$) system in an octahedral crystal field and spin-orbit coupling scheme among ^2E, $^2T_1$, $^2T_2$, $^4T_2$, and $^4T_1$. Arrows indicate transitions through spin-orbit coupling between the electronic states of Cr^3. (b) Configuration coordinate diagram in the harmonic approximation for the electronic states including spin-orbit coupling.

The vibronic Hamiltonian is written as

$$H(r,R) = -\frac{\hbar^2}{2M}\nabla_R^2 - \frac{\hbar^2}{2m}\nabla_r^2 + V_N(R) + V_{\mathrm{EP}}(r,R) + H_{\mathrm{SO}}(r,R) , \quad (1)$$

where M and m are effective nuclear and electronic masses, ∇_R^2 and ∇_r^2 operate on the nuclear collective coordinate R ($=\{R_j\}$) and electronic collective coordinate r ($=\{r_i\}$), and $V_N(R)$ is the harmonic potential, $V_{\mathrm{EP}}(r,R)$ is the electron-vibrational potential, and $H_{\mathrm{SO}}(r,R)$ is the spin-orbit coupling.[2] The terms $V_{\mathrm{EP}}(r,R)$ and $H_{\mathrm{SO}}(r)$ include electronic operators which mix different electronic states. In the BO adiabatic approximation, Eq. (1) separates into two equations, one associated with the electronic coordinates and the other with nuclear coordinates of the vibronic wave functions $\Psi_{in}(r,R)$ $[=\psi_i(r,R)\phi_{in}(R)]$: i.e.,

$$\left[-\frac{\hbar^2}{2m}\nabla_r^2 + V_N(R) + V_{\mathrm{EP}}(r,R) + H_{\mathrm{SO}}(r,R)\right]\psi_i(r,R) = \varepsilon_i(R)\psi_i(r,R) , \quad (2)$$

$$\left[-\frac{\hbar^2}{2M}\nabla_R^2 + \varepsilon_i(R)\right]\phi_{in}(R) = E_{in}\phi_{in}(R) , \quad (3)$$

where i and n represent electronic and vibrational states.

The terms of $V_{\mathrm{EP}}(r,R)$ and $H_{\mathrm{SO}}(r,R)$ may be expanded about the $R_j = 0$ nuclear equilibrium configuration, where the subscript j indicates the jth vibrational mode:[22,24]

$$V_{\mathrm{EP}}(r,R) = V_{\mathrm{EP}}^0(r) + \sum_j \frac{\partial V_{\mathrm{EP}}}{\partial R_j} R_j + (\text{higher-order terms}) , \quad (4)$$

$$H_{\mathrm{SO}}(r,R) = H_{\mathrm{SO}}^0(r) + \sum_j \frac{\partial H_{\mathrm{SO}}}{\partial R_j} R_j + (\text{higher-order terms}) . \quad (5)$$

The expanded vibrational modes may be classified as accepting modes and promoting modes:[22,26,27] The former is a sink for the electronic energy, and the latter induces electronic transitions. In cubic symmetry (e.g., $Y_3Al_5O_{12}$ crystal), the irreducible representations of the vibrational modes are Raman-active A_{1g}, E_g, and T_{2g} modes and iractive T_{1u} and T_{2u} modes. Since the A_{1g} breathing mode only shifts all the energy levels equally, it is ignored. The even-parity E_g and T_{2g} modes split and shift energy levels via the Jahn-Teller effect. In contrast, the odd-parity T_{1u}, and T_{2u} modes induce parity-forbidden transitions, as discussed in detail by Yamaga, Henderson, and O'Donnell.[28]

The electronic configurations of $^4T_2$ and $^4T_1$ in Cr^{3+} are t^2e. Since the spatial extent of the e orbital projects

out toward the neighboring ligand ions, these states undergo strong Jahn-Teller coupling. The E_g Jahn-Teller mode is dominant. On the other hand, the electron-vibrational coupling of the E_g Jahn-Teller mode for ^2E, $^2T_1$, and $^2T_2$ states, the electronic configurations of which are t^3, is very weak, as is confirmed by the observed sharp zero-phonon lines due to transitions between the ^2E, $^2T_1$, and $^2T_2$ excited states and the $^4A_2$ ground state. Although the T_{2g} Jahn-Teller mode mixes the different electronic states via the interactions $E\times T_1$, $E\times T_2$, and $T_1\times T_2$, the coupling coefficient is small compared with that of the E_g Jahn-Teller mode operating on the $^4T_2$ and $^4T_1$ states. Here we adopt the E_g mode as one accepting mode and the T_{2g} mode as one promoting mode denoted by subscripts a and p, respectively. The electronic wave function $\psi_i(r,R)$ in Eq. (2) is replaced by $\psi_i(r,R_a,R_p)$. The coupling coefficients $\partial V_{\rm EP}/\partial R_a$ for the accepting mode are set to a constant value A_i. Assuming that $H^0_{\rm SO}(r)\gg(\partial H_{\rm SO}/\partial R_p)R_p$, $(\partial V_{\rm EP}/\partial R_p)R_p$, and the higher-order terms of the electron-vibrational coupling are small and negligible, the electronic Hamiltonian [Eq. (2)] may be written as

$$\left[-\frac{\hbar^2}{2m}\nabla_r^2+V_N(R)+V^0_{\rm EP}(r)+A_iR_a+H^0_{\rm SO}(r)\right]\psi_i(r,R_a,0)=\varepsilon_i(R_a)\psi_i(r,R_a,0)\ . \tag{6}$$

The zeroth-order eigenvalues and eigenfunctions of Eq. (6) in the absence of $H^0_{\rm SO}(r)$ are represented by $\varepsilon^0_i(R_a)$ and $\psi^0_1(r,R_a,0)$, respectively. In a first-order calculation, we find the eigenfunction of Eq. (6) to be

$$\psi_i(r,R_a,0)=\psi^0_i(r,R_a,0)+\sum_k\frac{\langle\psi^0_k(r,R_a,0)|H^0_{\rm SO}(r)|\psi^0_i(r,R_a,0)\rangle}{\varepsilon^0_i(R_a)-\varepsilon^0_k(R_a)}\times\psi^0_k(r,R_a,0)\ , \tag{7}$$

where $\psi^0_i(r,R_a,0)$ and $\psi^0_k(r,R_a,0)$ are ^2E, $^4T_2$, $^4T_1$, $^2T_1$, and $^2T_2$ in Fig. 1(a). The eigenfunctions of Eq. (2), including the terms of $(\partial H_{\rm SO}/\partial R_p)R_p$ and $(\partial V_{\rm EP}/\partial R_p)R_p$ as perturbations, are represented by a linear combination of $\psi_i(r,R_a,0)$ and are given by

$$\psi_i(r,R_a,R_p)=\psi_i(r,R_a,0)+\sum_k\frac{\langle\psi_k(r,R_a,0)|(\partial H_{\rm SO}/\partial R_p+\partial V_{\rm EP}/\partial R_p)R_p|\psi_i(r,R_a,0)\rangle}{\varepsilon_i(R_a)-\varepsilon_k(R_a)}\psi_k(r,R_a,0)\ . \tag{8}$$

The vibrational wave functions of Eq. (3) are approximated by a product of harmonic-oscillator wave functions of accepting and promoting modes:

$$\phi_{in}(R)=\phi_{in'n''}(R)=\chi_{n'}(R_{ai})\chi_{n''}(R_{pi})\ ,\quad R_{ai}=R_a-\delta R_{ai},\quad R_{pi}=R_p\ ,\quad \delta R_{ai}=A_i/(M\omega^2)\ , \tag{9}$$

where n' and n'' are vibrational quantum numbers, δR_{ai} is a displacement from the equilibrium position for the accepting mode, and ω is the vibrational frequency of the accepting mode. Here we assume that the displacement for the promoting mode may be ignored.

We focus attention on the ^{2}E and $^4T_2$ vibronic states. The eigenfunctions and eigenvalues given in the form of diagonal matrix elements of Eq. (1) in the BO adiabatic approximation are

$$\Psi_{in}(r,R)=\psi_{in'n''}(r,R)=\psi_i(r,R)\phi_{in'n''}(R)\ , \tag{10}$$

$$E_{in}=E_{in'n''}=E_{i00}+n'\hbar\omega+n''\hbar\omega'\ , \tag{11}$$

where E_{i00} is the zero-phonon energy level of ith vibronic state and ω and ω' are vibrational frequencies of the accepting and promoting modes.

B. Mixing of $^4T_2$ into ^{2}E vibronic states

1. Zero-point vibration of accepting phonon mode

As the barrier separating the ^2E and $^4T_2$ vibronic states is lowered until it becomes comparable to the phonon energy, the adiabatic approximation becomes invalid and tunneling occurs between the two potential minima. Tunneling splitting 2δ, corresponding to the rate of tunneling between two zero-phonon states with the same energy, is calculated using Eqs. (8)–(10) and is given by

$$2\delta=\langle\Psi_{E00}(r,R)|\hbar\omega|\Psi_{T00}(r,R)\rangle=\hbar\omega\langle\psi_T(r,R)|\psi_E(r,R)\rangle\langle\chi_0(R_{aT})|\chi_0(R_{aE})\rangle\ . \tag{12}$$

When there is small energy separation $\Delta E=E(^4T_2)-E(^2E)$, the secular matrix including tunneling splitting is

$$\begin{array}{c|cc} & \Psi_{E00}(r,R) & \Psi_{T00}(r,R) \\ \Psi_{E00}(r,R) & 0 & \delta \\ \Psi_{T00}(r,R) & \delta & \Delta E \end{array}\ . \tag{13}$$

The ^2E lowest excited wave function mixed through tunneling[2-4] is

$$\Psi'_{E00}(r,R)=\Psi_{E00}(r,R)+\alpha\Psi_{T00}(r,R)\ , \tag{14}$$

$$\alpha=\frac{-2\delta}{\Delta E+[(\Delta E)^2+4\delta^2]^{1/2}}\ . \tag{15}$$

2. Break of adiabatic potential due to promoting phonon mode

The nonadiabatic terms ignored in the BO adiabatic approximation permit also mixing between different BO

eigenfunctions. The mixing due to the promoting phonon mode is dominant. The nonadiabatic Hamiltonian[23,26] is

$$H_{\mathrm{NA}}\Psi_{in'n''}(r,R)=-\frac{\hbar^2}{M}\frac{\partial\psi_i(r,R)}{\partial R_p}\frac{\partial\phi_{in'n''}(R)}{\partial R_p}\ , \tag{16}$$

where the term

$$-\frac{\hbar^2}{2M}\frac{\partial^2\psi_i(r,R)}{\partial R_p^2}\phi_{in'n''}(R)$$

is ignored. The off-diagonal matrix elements in Eq. (1) calculated using the ^2E and $^4T_2$ mixed-spin BO vibronic wave functions are

$$\langle\Psi_{Tn'n''}(r,R)|H_{\mathrm{NA}}|\Psi_{Em'm''}(r,R)\rangle=-\frac{\hbar^2}{M}\left\langle\psi_T(r,R)\left|\frac{\partial}{\partial R_p}\right|\psi_E(r,R)\right\rangle\left\langle\phi_{Tn'n''}(R)\left|\frac{\partial}{\partial R_p}\right|\phi_{Em'm''}(R)\right\rangle\ . \tag{17}$$

The electronic part in Eq. (17) is rewritten as

$$\left\langle\psi_T(r,R)\left|\frac{\partial}{\partial R_p}\right|\psi_E(r,R)\right\rangle=\frac{\langle\psi_T(r,R_a,0)|(\partial H_{\mathrm{SO}}/\partial R_p+\partial V_{\mathrm{EP}}/\partial R_p)|\psi_E(r,R_a,0)\rangle}{\varepsilon_E(R_a)-\varepsilon_T(R_a)}\ , \tag{18}$$

where a term representing a two-phonon process is ignored. The mixing between ^2E and $^4T_2$ electronic states occurs through spin-orbit and electron-vibrational couplings for the promoting mode as second-order perturbation. The vibrational part of Eq. (17) is

$$\left\langle\phi_{Tn'n''}(R)\left|\frac{\partial}{\partial R_p}\right|\phi_{Em'm''}(R)\right\rangle=\left\langle\chi_{n''}(R_{pT})\left|\frac{\partial}{\partial R_p}\right|\chi_{m''}(R_{pE})\right\rangle\langle\chi_{n'}(R_{aT})|\chi_{m'}(R_{aE})\rangle$$

$$=\left[\frac{M\omega'}{2\hbar}\right]^{1/2}(\sqrt{N_{m''}}\delta_{n'',m''-1}-\sqrt{N_{m''}+1}\delta_{n'',m''+1})\langle\chi_{n'}(R_{aT})|\chi_{m'}(R_{aE})\rangle\ , \tag{19}$$

$$\langle\chi_{n'}(R_{aT})|\chi_{m'}(R_{aE})\rangle=\exp\left[-\frac{S}{2}\right]\left[\frac{m'!}{n'!}\right]^{1/2}(\sqrt{S}\,)^{n'-m'}L_{m'}^{n'-m'}(S)\ , \tag{20}$$

$$N_{m''}=\frac{1}{\exp(\hbar\omega'/kT)-1},\quad \sqrt{S}=\sqrt{S_T}-\sqrt{S_E},\quad \hbar\omega S_i=A_i^2/2M\omega^2\ \ (i=E,t)\ , \tag{21}$$

where S_E and S_T are the Huang-Rhys parameters of the ^{2}E and $^4T_2$ excited vibronic states and $L_{m'}^{n'-m'}(S)$ are Laguerre polynomials.

At low temperatures the excited electron populates only the lowest zero-phonon level. Assuming that the lowest excited vibronic state is ^2E, Eq. (17) may be approximated by

$$\langle\psi_{Tn'1}(r,R)|H_{\mathrm{NA}}(r,R)|\Psi_{E00}(r,R)\rangle=R_{ET}\langle\chi_{Tn'}(R_{aT})|\chi_{E0}(R_{aE})\rangle\quad(n'=0,1,2,3,\ldots)\ . \tag{22}$$

The admixture coefficients $a_{n'}$ between $\Psi_{E00}(r,R)$ and $\Psi_{Tn'1}(r,R)$ are given approximately by first-order perturbation theory as

$$a_{n'}\simeq\frac{-\langle\Psi_{Tn'1}(r,R)|H_{\mathrm{NA}}(r,R)|\Psi_{E00}(r,R)\rangle}{E_{Tn'1}-E_{E00}}\ . \tag{23}$$

The value of the denominator [in Eq. (17)] is maximal at $n'\simeq S$, whereas that of the numerator is proportional to n'. The calculated coefficient a_0 in the case of Cr^{3+}:$Gd_3Sc_2Ga_3O_{12}$ (GSGG) is bigger than those of $a_{n'}$ $(n'\geq 1)$. The value of R_{ET} including the term $N_{m''}$ in Eq. (19) is estimated from the temperature dependence of the lifetime and the line shape of the luminescence.

In consequence, the ^2E lowest excited vibronic wave function of Eq. (1), mixed by both the zero-point vibration of the accepting mode and the nonadiabatic operator due to the promoting mode, is approximately given by a linear combination of $\Psi_{E00}(r,R)$ and $\Psi_{T0n''}(r,R)$ $(n''=0,1)$:

$$\Psi'_{E00}(r,R)=\Psi_{E00}(r,R)+\alpha\Psi_{T00}(r,R)+a_0\Psi_{T01}(r,T)\ . \tag{24}$$

In a previous paper, Yamaga, Henderson, and O'Donnell described the tunneling that occurs between the ^2E and $^4T_2$ zero-phonon levels in the presence of zero-point lattice vibrations around the equilibrium point at low temperature. The above treatment adds a nonadiabatic effect to the mixing of $^4T_2$ into ^2E vibronic states.

C. Line-shape function of an emission spectrum of Cr^{3+}

We consider the line shape of an emission spectrum derived from the probability of the transition from the ^2E lowest excited vibronic state $\Psi'_{E00}(r,R)$ in Eq. (24) to the $^4A_2$ ground state, $\Psi_{Am'm''}(r,R)$. The square of the electric dipole (magnetic dipole) matrix element between these states[29,30] is

$$W_{EA}=|\langle\Psi_{Am'm''}(r,R)|\mu|\Psi'_{E00}(r,R)\rangle|^2$$
$$=P_{EA}|\langle\phi_{Am'm''}(R)|\phi_{E00}(R)\rangle|^2+P_{TA}\{\alpha^2|\langle\phi_{Am'm''}(R)|\phi_{T00}(R)\rangle|^2+a_0^2|\langle\phi_{Am'm''}(R)|\phi_{T01}(R)\rangle|^2\}\ , \tag{25}$$

where

$$P_{iA}=|\langle\psi_A(r,R)|\mu|\psi_i(r,R)\rangle|^2\quad(i=E,T)\ .$$

The transition probability W_{EA}, obtained by substituting Eq. (20) into Eq. (25), is rewritten as

$$W_{EA}=P_{EA}\exp(-S_E)\frac{S_E^{m'}}{m'!}\delta_{m'',0}+P_{TA}\exp(-S_T)\frac{S_T^{m'}}{m'!}(\alpha^2\delta_{m'',0}+a_0^2\delta_{m'',1})\ . \tag{26}$$

The line-shape function of an emission spectrum at $T=0$ is

$$I(E)=I_0\sum_{m'm''}W_{EA}\delta(E-E_{E00}+E_{Am'm''})$$
$$=I_0\sum_{m'}\left[P_{EA}\exp(-S_E)\frac{S_E^{m'}}{m'!}\delta(E-E_{E00}+m'\hbar\omega)\right.$$
$$\left.+P_{TA}\exp(-S_T)\frac{S_T^{m'}}{m'!}\{\alpha^2\delta(E-E_{E00}+m'\hbar\omega)+a_0^2\delta(E-E_{E00}+m'\hbar\omega+\hbar\omega')\}\right]\ , \tag{27}$$

where E_{E00} is given in Eq. (11) and the zero-phonon energy E_{A00} is set equal to 0. The zero-phonon lines from the first and second terms in Eq. (27) are located at $E=E_{E00}$, wheras the lines from the third term are shifted to lower energy by $\hbar\omega'$, associated with phonon emission of the promoting mode. Therefore the line-shape function is the superpostion of the R line and its phonon sideband due to the weak vibronic coupling of the state $\Psi_{E00}(r,R)$ and the broadband due to the strong vibronic coupling of the states $\Psi_{T00}(r,R)$ and $\Psi_{T01}(r,R)$ with an intensity ratio of $P_{EA}:(\alpha^2+a_0^2)P_{TA}$.

The emission spectrum represented by Eq. (27) consists of a sum of δ functions. There is some distribution of the vibrational frequencies of the accepting mode. Pryce[30] has developed the line shape taking account of the distribution $\rho(E)$. We describe this method briefly assuming that the couplings S_E and S_T are constant in the energy range of $\rho(E)$. The modified function is

$$I(E)=I_0\sum_{m'}\left[P_{EA}\exp(-S_E)\frac{S_E^{m'}}{m'!}B_{m'}(E)\right.$$
$$+P_{TA}\exp(-S_T)\frac{S_T^{m'}}{m'!}$$
$$\left.\times\{\alpha^2B_{m'}(E)+a_0^2B_{m'}(E+\hbar\omega)\}\right]\ , \tag{28}$$

where the function $B_{m'}(E)$ is the line shape for an m'-phonon process. For $m'=0$, $B_0(E)$ is the zero-phonon line-shape function. The function is a Gaussian rather than Lorentzian because there is a distribution of random strain in real crystals. Accordingly, we write

$$B_0(E)=N_0\exp\left[-\frac{(E-E_{E0})^2}{2\Delta_0^2}\right]\ , \tag{29}$$

where N_0 is a normalization factor and Δ_0 is a width. The emitted phonon spectrum is approximated by the sum of Gaussians with mean phonon energy $\hbar\omega_k$:

$$\rho(E)=N_\rho\sum_k\alpha_k\exp\left[-\frac{(E+\hbar\omega_k)^2}{2\Delta_{1k}^2}\right]\ , \tag{30}$$

where α_k is a constant value, Δ_{1k} a width, and N_ρ a normalization factor. The line-shape functions $B_{m'}(E)$ for higher-order processes are obtained by performing an m'-times convolution with the pnonon spectrum $\rho(E)$:

$$B_{m'}(E)=\int_0^\infty B_{m'-1}(E')\rho(E-E')dE'\quad(m'\geq1)\ . \tag{31}$$

The convolution of a Gaussian with a Gaussian is a Gaussian. Assuming that $\rho(E)$ is a single Gaussian, the function is

$$B_{m'}(E)=N_{m'}\exp\left[-\frac{(E-E_{m'})^2}{2\Delta_{m'}^2}\right]\ , \tag{32}$$

where

$$E_{m'}=E_{E00}-m'\hbar\omega \tag{33}$$

and

$$\Delta_{m'}^2=\Delta_0^2+m'\Delta_1^2\ . \tag{34}$$

III. EXPERIMENTAL PROCEDURE AND RESULTS

The GSAG and GSGG single crystals were grown from high-purity oxides using the Czochralski technique,[6] whereas the YGG samples were thin films grown by rf sputtering.[31] The growth processes of these mixed garnet materials may be controlled to give various degrees of compositional disorder. The different garnet compositions were estimated by the energy-dispersed x-ray spectra detected with an x-ray microanalyzer. The compositions of the mixed garnet crystals used in this

study were $Y_{3.1}Ga_{4.9}O_{12}$ (YGG1), $Y_{3.8}Ga_{4.2}O_{12}$ (YGG2), $Gd_3Sc_{2.2}Al_{2.8}O_{12}$ (GSAG), and $Gd_3Sc_{1.9}Ga_{3.1}O_{12}$ (GSGG). The deviation from the $A_3B_5O_{12}$ or $A_3B_2C_3O_{12}$ stoichiometric composiion is manifest as *structural disorder,* which influences the shape of the R lines in Cr^{3+}-doped garnet crystals.[1,6] The luminescence spectra from the samples were excited using the 488-nm line from an Ar^+ laser and detected using a GaAs photomultipler tube at the exit slit of a 1-m grating monochromator. In fluoresence line narrowing (FLN), a narrow laser line is tuned to wavelengths in the inhomogeneously broadened R_1 lines. The samples were mounted in a closed-cycle refrigerator with temperature controlled to ± 0.1 K in the range 10–300 K.

Figure 2 shows the cw emission spectra of Cr^{3+}-doped YGG1, YGG2, GSAG, and GSGG at 10 K.[2,6,7] In YGG1 and YGG2, the Cr^{3+} ions occupy a strong octahedral crystal-field site, so that at low temperature ($T < 50$ K) the emission is due to the R line and its phonon sideband with a fairly weak broadband observed at longer wavelengths. The integrated intensity ratio (I_T/I_E) of the broadband to the R line and its phonon sideband is 0.4 for YGG1 and 1 in YGG2. This is explained in terms of the nonstoichiometry of samples YGG1 and YGG2 in which Y^{3+} ions with larger ionic radius replace the smaller Ga^{3+} ions in octahedral sites.[31] The replacement decreases the crystal field of the Cr^{3+} ion, the strength of which reflects the distance between the central Cr^{3+} ion and six nearest-neighbor O^{2-} ions.[14] The crystal field of Cr^{3+}:GSAG and Cr^{3+}:GSGG is intermediate, the ^2E and $^4T_2$ levels being close together in energy. The energy separation ($\Delta E = E_{T0} - E_{E0}$) is 50–110 cm^{-1}.[1,3,5,10] The superposition of the broadband on the R line and its phonon sideband in Cr^{3+}:GSGG is observed even at 1.6 K, where the thermal energy k_BT is fairly small relative to the energy separation. The ratios of I_T/I_E for GSAG and GSGG are ~5. These experimental results indicate that the mixing of the $^4T_2$ second excited vibronic state into the ^2E lowest excited vibronic state occurs through spin-orbit coupling in the nonadiabatic Hamiltonian.

Figure 3(a) shows the phonon structure of the emission

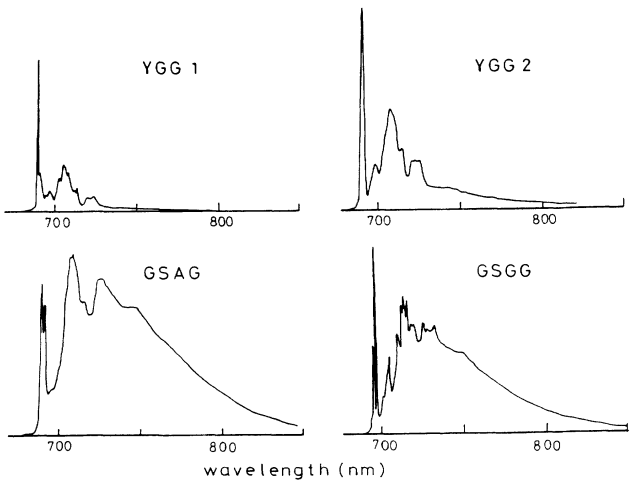

FIG. 2. Emission spectra of Cr^{3+}-doped $Y_{3.1}Ga_{4.9}O_{12}$ (YGG1), $Y_{3.8}Ga_{4.2}O_{12}$ (YGG2), $Gd_3Sc_{2.2}Al_{2.8}O_{12}$ (GSAG), and $Gd_3Sc_{1.9}Ga_{3.1}O_{12}$ (GSGG) at 10 K with excitation using the 488-nm resonance line from an Ar^+-ion laser.

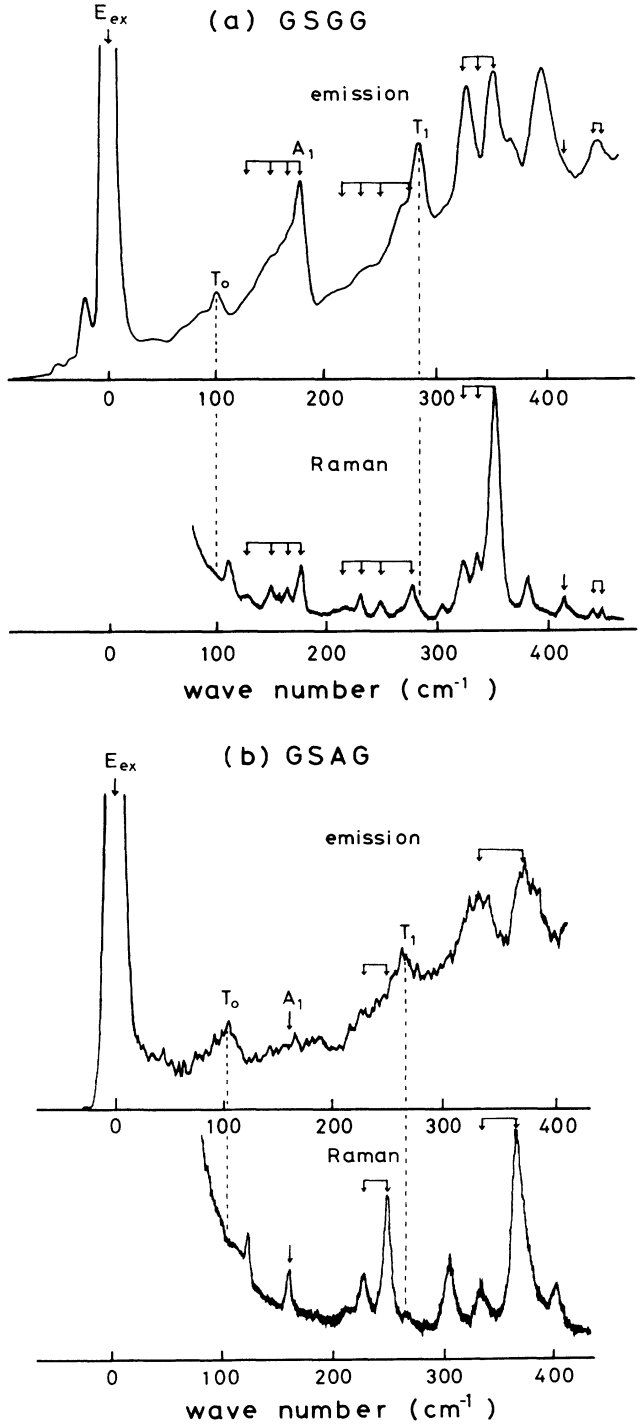

FIG. 3. Fluoresence line narrowing of Cr^{3+} ions compared with Raman spectra at 300 K: (a) GSGG at 10 K excited in the $R_1(a)$ line at 696.6 nm and (b) GSAG at 4.2 K excited in the R_1 line at 692.7 nm. The energy origin of emission spectra is the excitation energy.

of Cr^{3+}:GSGG observed at 10 K with excitation of 696.6 nm resonant with the $R_1(a)$ line[6,7] and the Raman spectrum at 300 K. The horizontal scale is changed to a wave number in order to compare the emission spectrum with the Raman spectrum. The origion is 14 355 cm^{-1} of excitation energy. The R_1 line is accompanied by its phonon replica. The arrows indicate that the phonon energies between the emission and Raman spectra are equal to each other. The phonon energy (100 cm^{-1}) of the emission spectrum is shifted to lower energy from that (113 cm^{-1}) of the Raman spectrum. It may be due to phonon coupling with the excited state. The phonon spectrum around 178, 278, and 355 cm^{-1} is the accepting phonon modes. The sharp line denoted by T_0 and T_1 are separated in energy by 186 cm^{-1}, which is nearly equal to the phonon energy (178 cm^{-1}) denoted by A_1. The intensity ratio of the T_0 and T_1 lines is about 1:4. The T_0 and T_1 lines may be assigned as the zero- and one-phonon lines, respectively, due to the $^4T_2 \rightarrow {}^4A_2$ transition assisted by the promoting phonon mode. Equation (28) indicates that the zero-phonon energy of the broadband is shifted to lower energy from the R_1 zero-phonon line by an amount equal to the energy $\hbar\omega'$ of the promoting phonon. Similar spectra were observed in Cr^{3+}:GSAG, as shown in Fig. 3(b). The energy origin is 14 441 cm^{-1}. The phonon energy (104 cm^{-1}) of the emission spectrum is also shifted to lower energy from that (122 cm^{-1}) of the Raman spectrum. The energy separation (161 cm^{-1}) between T_0 and T_1 is very close to that (160 cm^{-1}) of the accepting phonon mode denoted by A_1.

The temperature dependence of R-line spectra of Cr^{3+}:GSGG excited with 488 nm from an Ar-ion laser was measured. The line shape of the R_1 line observed at 10 K fitted a Gaussian due to an inhomogeneous broadening. The width Δ_0 in Eq. (29) was 6 cm^{-1}. Increasing the temperature broadens the R_1 line. The temperature dependence of the width is assumed to be $[\Delta_{obs}(T)]^2=\Delta_0^2+[\Delta_0(T)]^2$ and $\Delta_{obs}(10)=\Delta_0$. The values of $\Delta_{obs}(T)$ and $\Delta_0(T)$ at temperature T are summarized in Table I.

Figure 4 shows the temperature dependence of the emission spectra of Cr^{3+}:GSAG. The linewidths of R lines and their phonon sidebands are broadened, and the broadband is enhanced with the increase of temperature. The integrated intensities of the emission spectra are almost constant up to 300 K. The lifetime and intensities of Cr^{3+}:GSAG (Ref. 17) and Cr^{3+}:GSGG (Refs. 16 and 17) were decreased abruptly above 500 K.

TABLE I. Linewidth of R_1 line of Cr^{3+}:GSGG.

Temperature T (K)	Width (cm^{-1}) $\Delta_{obs}(T)$	Δ_0	$\Delta_0(T)$
10	6	6	0
30	6	6	0
45	7	6	4
60	9	6	7
70	18	6	17
90	22	6	21
120	42	6	42
176	50	6	50

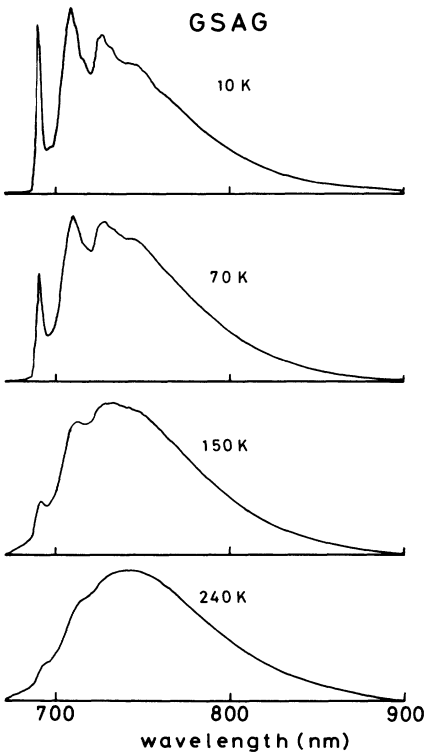

FIG. 4. Temperature dependence of the emission spectra of Cr^{3+}-doped $Gd_3Sc_{2.2}Al_{2.8}O_{12}$ (GSAG) with excitation using the 488-nm resonance line from an Ar-ion laser.

IV. COMPARISON OF EXPERIMENTAL RESULTS WITH THEORY

We calculate the line shape using Eq. (28) to compare with the observed spectra in Cr^{3+}:YGG1, Cr^{3+}:YGG2, Cr^{3+}:GSAG, and Cr^{3+}:GSGG in Fig. 2. Equation (28) includes terms of both zero-point vibration of the accepting mode and the breakdown of the adiabatic potential caused by the promoting mode. The former is independent of temperature, whereas the latter includes the temperature dependence of the mixing coefficient a_0 multiplied by a factor of $N_{m'}+1$. Which mode is dominant for the broadband is determined experimentally. Here we assume that the promoting mode effect is dominant, taking account of FLN measurements (Fig. 3) and temperature dependence of the luminescence (Fig. 4) of Cr^{3+}:GSGG and Cr^{3+}:GSAG.

First, we estimate the physical parameters in Eq. (20): We determine $S_T=5.5$ and $S_E=0.5$ from the line-shape analysis of the broadband due to the $^4T_2 \rightarrow {}^4A_2$ transition and of the R line and its phonon sideband due to the $^2E \rightarrow {}^4A_2$ transition in the case of Cr^{3+}:GSGG. The electronic transition probabilities P_{EA} and P_{TA} are estimated from the lifetime of the Cr^{3+} luminescence. The lifetime of the R line of Cr^{3+}:$Y_3Al_5O_{12}$ (YAG) associated with Cr^{3+} ions in a strong crystal field is $\simeq 8$ ms at 4 K,[9]

whereas that of the broadband of Cr^{3+}:$La_3Lu_2Ga_3O_{12}$ (LLGG) with a weak crystal field is $\simeq 150\ \mu s$ at 4 K.[4] As P_{EA} and P_{TA} are the inverse of the lifetimes, the ratio P_{EA}:P_{TA} is 1:50. The linewidths [full width at half maximum (FWHM)] of the zero-phonon R lines observed in YGG1, YGG2, GSAG, and GSGG are in the range 10–50 cm^{-1}. The large widths observed in YGG2 and GSAG are caused by disorder due to the nonstoichiometric composition of mixed garnet crystals. The value of Δ_0 is 20 cm^{-1}. The accepting phonon spectrum $\rho(E)$ is determined from the observed phonon sideband due to the transition $^2E \rightarrow {}^4A_2$. The phonon structure in YGG1 and GSGG is resolved, whereas that in YGG2 and GSAG is unresolved. Then the accepting phonon spectrum for the ^2E state is approximated by the sum of four Gaussian with $\hbar\omega_1 = 180$ cm^{-1}, $\hbar\omega_2 = 380$ cm^{-1}, $\hbar\omega_3 = 520$ cm^{-1}, and $\hbar\omega_4 = 720$ cm^{-1} with $\alpha_1:\alpha_2:\alpha_3:\alpha_4 = 0.1:0.7:0.12:0.08$ in Eq. (30), whereas that for the $^4T_2$ state is a single Gaussian with $\hbar\omega_1 = 180$ cm^{-1}. The promoting phonon energy $\hbar\omega'$ is 100 cm^{-1}. The widths Δ_1 of these Gaussian distributions are nearly equal to 50 cm^{-1}.

Figure 5 shows the line shapes at $T = 0$ calculated using Eq. (28), the estimated physical values, and different values of mixing parameter a_0^2. The origin of the calculated line shape is set to the energy (690 nm) of the R_1 lines of Cr^{3+}:YGG2 and Cr^{3+}:GSAG. The intensity of the experimental zero-phonon emission line may be reduced because of the reabsorption. The reduction factor

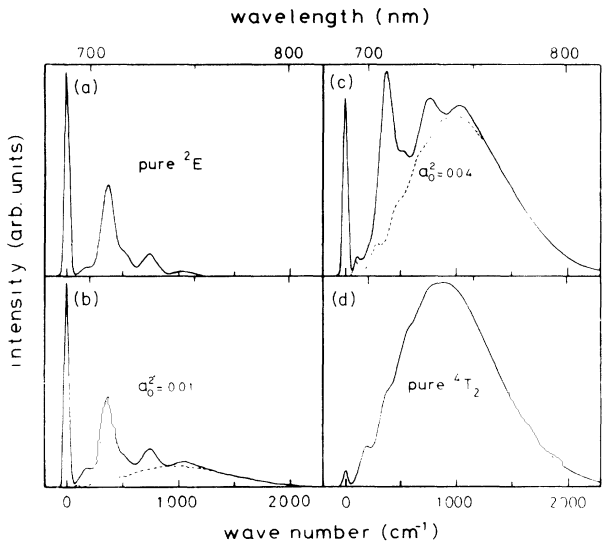

FIG. 5. Calculated line shapes of the Cr^{3+} luminescnece due to transitions from (a) the pure ^2E lowest excited state ($a_0^2 = 0$), (b) the lowest excited stated mixed between ^2E and $^4T_2$ vibronic states with mixing parameter $a_0^2 = 0.01$, (c) the mixed lowest excited state with $a_0^2 = 0.04$, and (d) the pure $^4T_2$ lowest excited state. Dotted curves represent the contribution from a fraction of the $^4T_2$ vibronic state in the lowest excited state. The origin of the calculated line shape in (a), (b), and (c) takes the energy (690 nm) of the R_1 lines of Cr^{3+}:YGG2 and Cr^{3+}:GSAG, whereas that in (d) takes the energy of the zero-phonon line from the $^4T_2 \rightarrow {}^4A_2$ transition.

is defined as R. Figure 5(a) shows the line shape due to a transition from a pure ^2E lowest excited vibronic state, corresponding to $a_0^2 = 0$, with a reduction factor $R = 0.3$. The line shape calculated using $a_0^2 = 0.01$ and $R = 0.3$ [Fig. 5(b)] fits the observed spectrum of Cr^{3+}:YGG2. The broadband is gradually enhanced as the mixing parameter a_0^2 increases. The line shape calculated using $a_0^2 = 0.04$ and $R = 0.18$ [Fig. 5(c)] fits the observed spectrum of Cr^{3+}:GSAG. The line shape due to a transition from the pure $^4T_2$ lowest vibronic state [Fig. 5(d)] is appropriate to the observed spectra of Cr^{3+}:$La_3Lu_2Ga_3O_{12}$ (Ref. 4) and Cr^{3+}:$ZnWO_4$.[8,32] The values of a_0^2 calculated for YGG2 and GSAG are small compared with those ($a_0^2 = \beta^2/\alpha^2 = 0.02$, 0.1) estimated from the temperature dependence of the intensity ratio I_T/I_E.[2] The difference may be due to the estimation of I_T/I_E because it is difficult to separate accurately the different parts of the $^2E \rightarrow {}^4A_2$ and $^4T_2 \rightarrow {}^4A_2$ transitions in the observed emission spectra.

The temperature dependence of the line shape of the luminescence and the decay times including the effect of radiationless transitions between the excited states and between the excited and ground states is very important for laser operations. The radiationless relaxation processes and energy migration in alexandrite,[33,34] emerald,[35] and garnet crystals[12,36] have been studied by laser-induced grating spectroscopy. The dephasing time T_2, corresponding to radiationless relaxation processes from the $^4T_2$ to the ^2E states, is 33 fs for GSGG crystals.[12] The processes involve internal conversion (IC) and intersystem crossing (ISC). The radiationless relaxation to the ^2E level through intersystem crossing is dominant. The ratio $K_{NR}(ISC)/K_{NR}(IC)$ of the nonradiative decay rates for the two processes was estimated to be 2.2 for the $^4T_2$ band excitation of Cr^{3+}:GSGG.[36] As the temperature increases, radiationless transitions from the lowest excited state to the ground state occur.[25] The process reduces the quantum efficiency of the luminescence. The observed integrated intensities of the luminescence for Cr^{3+}:GSAG and Cr^{3+}:GSGG are nearly constant below 300 K. The behavior of the spectra measured for Cr^{3+}:GSGG in the range 77–600 K indicates luminescence quenching above 500 K.[16]

We consider the temperature dependence of the line shape of the luminescence for Cr^{3+}:GSAG, taking account of the above radiationless processes: The electron excited into the $^4T_1$ or $^4T_2$ band relaxes nonradiatively to the lowest excited state through intersystem crossing. The effect of radiationless transitions to the ground state are neglected below room temperature. Increasing temperature broadens the emission lines and excites population in the higher excited electron levels. The contribution from temperature of the R-line width of Cr^{3+}:GSGG is estimated and summarized in Table I. The higher excited levels consist of the ^2E vibronic levels with dominant frequency 380 cm^{-1} and the $^4T_2$ vibronic levels with a single frequency 160–180 cm^{-1} for Cr^{3+}:GSGG and Cr^{3+}:GSAG. The energy separation between ^2E and $^4T_2$ zero-phonon levels for Cr^{3+}:GSAG was estimated to be 150 cm^{-1} from the temperature

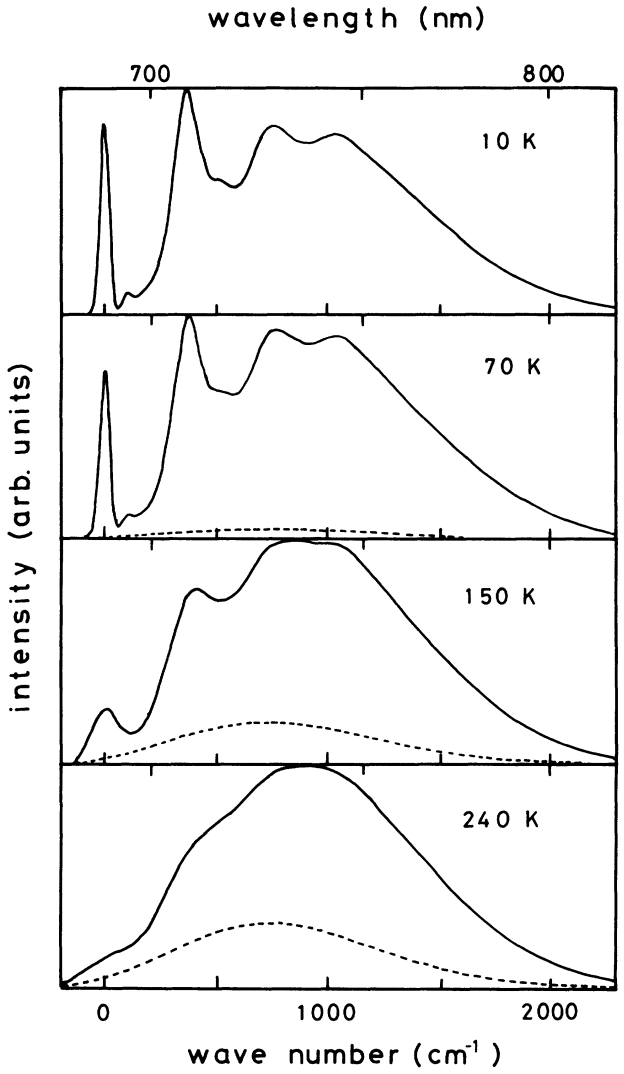

FIG. 6. Line shapes of the luminescence calculated as a function of temperature. The solid and dotted lines represent the whole spectra and the component contributed from the second excited state $\Psi'_{T00}(r,R)$, respectively.

dependence of the intensity ratio I_T/I_E.[2] Here we assume that the excited electron populates only the second excited zero-phonon level associated with the wave function

$$\Psi'_{T00}(r,R)=\Psi_{T00}(r,R)-\alpha\Psi_{E00}(r,R)$$

and that the population to the higher vibronic levels $\Psi'_{En'n''}(r,R)$ and $\Psi'_{Tn'n''}(r,R)$ is neglected below 300 K. Figure 6 shows the line shape of the luminescence calculated with a simple contribution from two ^2E and $^4T_2$ zero-phonon levels as a function of temperature. The solid and dotted lines represent the whole spectra and the components contributed from the second excited state $\Psi'_{T00}(r,R)$, respectively. The calculated line shapes of the luminescence agree with the observed spectra of Cr^{3+}:GSAG in Fig. 4.

The enhancement of the broadband emission with the increase of temperature has been calculated in terms of the temperature dependence of the mixing parameter a_0 produced by the promoting mode and thermal population of the second excited zero-phonon level. Donnelly *et al.*[10] and others,[5] have discussed a shift of $^4T_2$ levels to lower energy due to lattice dilation with the increase of temperature. Increasing temperature, the energy separation ΔE between ^2E and $^4T_2$ states is reduced so that thermal population to $^4T_2$ occurs easily at lower temperature. However, it is very difficult to distinguish experimentally between them.

V. CONCLUSIONS

The breakdown of the ^2E and $^4T_2$ adiabatic vibronic states of Cr^{3+}, the energy levels of which are very close, occurs through spin-orbit coupling and the nuclear kinetic-energy operators. This effect shows up in the emission spectra of Cr^{3+} ions in garnet crystals (e.g., Cr^{3+}:GSAG, GSGG). Even at $T<30$ K, where the thermal energy is fairly small compared with the energy separation between ^2E and $^4T_2$ levels, the experimental emission line shape is composed of the R line with the phonon sideband associated with the $^2E\rightarrow{}^4A_2$ transition and the broadband $^4T_2\rightarrow{}^4A_2$ transition. The calculated emission line shapes due to the transition from the lowest excited vibronic state mixed by spin-orbit coupling and nuclear kinetic-energy operators agree fairly well with the observed emission spectra in Cr^{3+}:YGG1, Cr^{3+}:YGG2, Cr^{3+}:GSAG, and Cr^{3+}:GSGG. The calculated temperature dependence of the line shape also agrees with that of the observed spectra for Cr^{3+}:GSAG.

ACKNOWLEDGMENTS

This program of research was supported by the SERC through research Grants Nos. GR/D/23534, GR/D/62670, and GR/E/77557 and from the Ministry of Education through a Science Research Grant-in-Aid (03650032). The authors thank Professor H. Shimizu for the measurement of the Raman spectra in GSAG and GSGG. One of the authors (M.Y.) thanks Dr. M. Aoki for valuable discussions.

[1]B. Struve and G. Huber, Appl. Phys. B **36**, 195 (1985).
[2]M. Yamaga, B. Henderson, and K. P. O'Donnell, J. Phys. Condens. Matter **1**, 9175 (1989).
[3]M. Yamaga, B. Henderson, K. P. O'Donnel, C. Trager-Cowan, and A. Marshall, Appl. Phys. B **50**, 425 (1990).
[4]M. Yamaga, B. Henderson, K. P. O'Donnell, and Y. Gao, Appl. Phys. B **51**, 132 (1990).
[5]B. Henderson, A. Marshall, M. Yamaga, K. P. O'Donnell, and B. Cockayne, J. Phys. C **21**, 6187 (1988).
[6]A. Marshall, K. P. O'Donnell, M. Yamaga, B. Henderson, and B. Cockayne, Appl. Phys. A **50**, 565 (1990).
[7]K. P. O'Donnell, A. Marshall, M. Yamaga, B. Henderson, and B. Cockayne, J. Lumin. **42**, 365 (1989).
[8]M. Yamaga, A. Marshall, K. P. O'Donnell, and B. Henderson,

J. Lumin. **47**, 65 (1990).
[9]J. P. Hehir, M. O. Henry, J. P. Larkin, and G. F. Imbusch, J. Phys. C **7**, 2241 (1974).
[10]C. J. Donnelly, S. M. Healy, T. J. Glynn, G. F. Imbusch, and G. P. Morgan, J. Lumin. **42**, 117 (1988).
[11]C. J. Donnelly, T. J. Glynn, G. P. Morgan, and G. F. Imbusch, J. Lumin. **48&49**, 283 (1991).
[12]A. Suchocki and R. C. Powell, Chem. Phys. **128**, 59 (1988).
[13]W. Nie, G. Boulon, and A. Monteil, J. Phys. (Paris) **50**, 3309 (1989).
[14]S. Sugano, Y. Tanabe, and H. Kamimura, *Multiplets of Transition Metals in Crystals* (Academic, New York, 1970).
[15]S. Sugano, A. L Schawlow, and F. Varsanyi, Phys. Rev. **120**, 2045 (1960).
[16]G. Armagan and B. Di Bartolo, in *Tunable Solid-State Lasers II*, edited by A. B. Budgeor, L. Esterowitz, and L. G. DeShazer (Springer-Verlag, Berlin, 1986), pp. 35–43.
[17]L. J. Andrews, S. M. Hitelman, M. Kokta, and D. Gabbe, J. Chem. Phys. **84**, 5229 (1986).
[18]S. Payne, L. L. Chase, H. W. Newkirk, L. K. Smith, and W. F. Krupke, IEEE J. Quantum Electron. **QE-24**, 2243 (1988).
[19]B. Barnett and R. Englman, J. Lumin **3**, 37 (1970); see also R. Englman and B. Barnett, J. Lumin. **3**, 55 (1970).
[20]T. Azumi, Chem. Phys. Lett. **25**, 135 (1974).
[21]N. Shimakura, Y. Fujimura, and T. Nakajima, Chem. Phys. Lett. **40**, 222 (1976).
[22]S. H. Lin, J. Chem. Phys. **44**, 3759 (1966); see also S. H. Lin and R. Bersohn, J. Chem. Phys. **48**, 2732 (1968).
[23]M. Bixon and J. Jortner, J. Chem. Phys. **48**, 715 (1968).
[24]B. R. Henry and W. Siebrand, J. Chem. Phys. **54**, 1072 (1971).
[25]R. Englman, *Non-radiative Decay of Ions and Molecules in Solids* (North-Holland, Amsterdam, 1979).
[26]F. Auzel, in *Luminescence of Inorganic Solids*, edited by B. Di Bartolo (Plenum, New York, 1978), pp. 67–113.
[27]R. H. Bartram and A. M. Stoneham, Solid State Commun. **17**, 1593 (1975).
[28]M. Yamaga, B. Henderson, and K. P. O'Donnell, J. Lumin. **46**, 397 (1990).
[29]B. Henderson and G. F. Imbusch, *Optical Spectrsocopy of Inorganic Solids* (Clarendon, Oxford, 1989), Chap. 5.
[30]M. H. L. Pryce, in *Phonon*, edited by R. W. Stevenson (Oliver&Boyd, Edinburgh, 1966), pp. 403–448.
[31]M. Yamaga, A. Marshall, K. P. O'Donnell, B. Henderson, and Y. Miyazaki, J. Lumin. **39**, 335 (1988).
[32]W. Kolbe, K. Petermann, and G. Huber, IEEE J. Quantum Electron. ***QE*-21**, 1596 (1985).
[33]A. Suchocki, G. D. Gilliland, and R. C. Powell, Phys. Rev. B **35**, 5830 (1987).
[34]G. D. Gilliland, A. Suchocki, K. W. Ver Steeg, and R. C. Powell, Phys. Rev. B **38**, 6227 (1988).
[35]G. J. Quarles, A. Suchocki, and R. C. Powell, Phys. Rev. B **38**, 9996 (1988).
[36]F. M. Hashmi, K. W. Ver Dteeg, F. Durville, and R. C. Powell, Phys. Rev. B **42**, 3818 (1990).